Distance-dependent noise measurements in scanning force microscopy

1996 J. Phys.: Condens. Matter 8 7561

(http://iopscience.iop.org/0953-8984/8/41/006)

J. Phys.: Condens. Matter **8** (1996) 7561–7577. Printed in the UK

Distance-dependent noise measurements in scanning force microscopy

Andreas Roters and Diethelm Johannsmann

Max Planck Institute for Polymer Research, PO Box 3148, 55021 Mainz, Germany

Received 18 April 1996, in final form 4 July 1996

Abstract. The changes in the thermal noise spectrum of a scanning-force-microscope cantilever upon approach of the tip to the sample were used to investigate the interactions between the cantilever and the sample. The investigation of thermal noise is the natural choice for dynamic measurements with little disturbance of the sample. In particular, the small amplitudes involved ensure linear dynamic response. It is possible to discriminate between viscous coupling, elastic coupling and changes in the effective mass. The technique is versatile in terms of substrates and environments. Hydrodynamic long-range interactions depending on the sample, the geometry and the ambient medium are observed. The dependence of hydrodynamic interaction on various parameters such as the viscosity and the density of the medium is described. For sufficiently soft surfaces, the method is sensitive to viscoelastic properties of the surface. For example, the viscous coupling to the surface is strongly increased when the surface is covered with a swollen 'polymer brush'.

1. Introduction

Recently there has been much interest in the use of scanning force microscopy (SFM) to map the dynamical properties of surfaces. Several techniques based on SFM [1] were developed to sense viscoelastic properties of the sample. Most approaches are variations of 'force modulation microscopy'. For example, the slope of the force–distance curve in the repulsive force region was measured by oscillating the sample sinusoidally in height. The in-phase and the out-of-phase deflection of the cantilever correspond to elastic and viscous coupling to the surface respectively [2–5]. The tapping mode has also been used to derive the local compliance [6]. Florin *et al* [7] have modulated the force by attaching a small magnet to the tip and modulating the magnetic field in the chamber. In this paper we report initial progress using an alternative scheme.

Instead of actively modulating the cantilever and observing the response, we analyse the distance dependence of the thermal noise. The thermal noise is Brownian motion of the cantilever. It is connected to the local mechanical compliance via the fluctuation–dissipation theorem. In this respect, our approach is equivalent to schemes where active modulation is employed. The difference lies in the average amplitude of displacement and in the strength of the forces involved. For a cantilever with a spring constant of 0.1 N m^{-1}, the noise amplitude at the resonance is about $\langle u(\omega)^2\rangle^{1/2} \approx 0.01$ Å $Hz^{-1/2}$. The integrated RMS displacement is $\langle u^2\rangle^{1/2} \approx 2$ Å.

We find strong hydrodynamic effects at distances from the sample surface of up to 30 μm. Given the long range of the hydrodynamic interaction, it probably prevents local measurements on the molecular scale. One possibility for circumventing hydrodynamic

0953-8984/96/417561+17$19.50

interactions is of course to measure in vacuum. This mode unfortunately excludes many samples of interest such a biological tissue in an aqueous environment, polymeric adsorbates and any kind of film with a high vapour pressure. Working in a liquid environment also is desirable when weak forces are involved. In liquids, the van der Waals forces are weaker than in gaseous media. Therefore many dynamical investigations of practical interest have to deal with hydrodynamics. They are very important for understanding the dynamical modes of the scanning force microscope. In many cases such as polymeric stabilizers for colloids, the hydrodynamic interaction itself is of immediate interest, because it determines the rheological behaviour of the bulk dispersion. In other cases, hydrodynamic interaction may be an impediment to dynamical studies on the sample itself. In these cases, a detailed modelling of the hydrodynamic contribution is still essential in order to determine properly the dynamic properties of the sample itself.

Apart from modelling the hydrodynamic interactions, it seems worthwhile to seek strategies to minimize them. As we shall show below, the two options are firstly to use cantilevers, which are sharply pointed on the scale of tens of microns (like glass fibres) or secondly to approach the sample from the side instead of from below so that the dynamical interactions mainly involve shear strain rather than compression.

Although imaging itself is a minor issue in this context, our experimental procedure may prove useful in the imaging of very soft samples. Soft surfaces are in general hard to image with the force microscope because of indentation of the cantilever into the surface. The non-contact mode has been shown to avoid some of the problems. Probing the hydrodynamic interaction may be an alternative approach. Although these measurements are intrinsically slow, the contrast mechanism is different from the contrast in the non-contact mode. There is conceptual similarity to the scanning near-field acoustic microscope [8, 9]. However, we do not actively modulate and work at much lower amplitudes.

As we show in section 3, the dynamical response of the cantilever to the presence of the sample markedly depends on the viscoelastic properties of the surface. When comparing surfaces coated with polymer brushes with bare glass surfaces, we find a distance range of very high friction and even an increased spring constant, which is not present on the glass surface. In this way we have a local probe for hydrodynamic interactions which otherwise have to be inferred in a much more indirect way, e.g. from the dynamic behaviour of a dispersion of spheres coated with analogous polymer bushes.

2. Theory

We are only interested in mechanical noise. Around the resonance frequency, the noise is dominated by thermally induced lever noise [10–12]. The Brownian motion of an elastically suspended body in a fluid is treated in the textbooks (see e.g. [13, 14]). Figure 1 depicts the model.

Here, we follow the treatment by Reichl [13]. We start from the Langevin equation

$$\frac{\mathrm{d}^2u}{\mathrm{d}t^2} + \gamma\frac{\mathrm{d}u}{\mathrm{d}t} + \omega_0^2 u = \frac{1}{m}R(t) \tag{1}$$

where u is the displacement, $\omega_0 = (\kappa/m)^{1/2}$ the eigenfrequency, γ the damping constant, κ the spring constant, m the mass and $R(t)$ the random force. The power spectrum of the random force does not depend on frequency ('white noise'). The parameters γ, ω_0 and m are effective parameters, which are not necessarily properties of the cantilever alone. In the

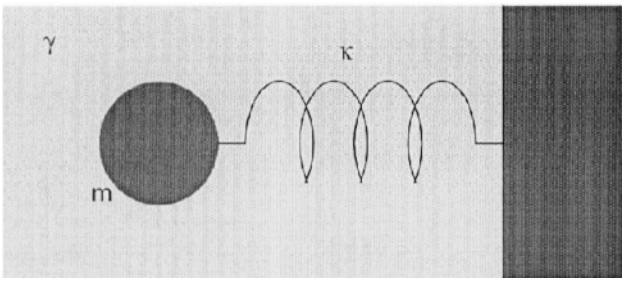

Figure 1. The dynamical model of a cantilever immersed in a viscous medium and suspended by an elastic spring.

following, we perform a harmonic analysis. In the frequency domain, equation (1) becomes

$$(-\omega^2 - \mathrm{i}\gamma\omega + \omega_0^2)u(\omega) = \frac{1}{m}R(\omega) \tag{2}$$

where we have adopted the convention that all time-dependent quantities vary as $\exp(-\mathrm{i}\omega t)$.

The susceptibility $\chi = \chi' + \mathrm{i}\chi''$ is given by

$$\chi(\omega) = \frac{u(\omega)}{R(\omega)} = \frac{1}{m(-\omega^2 - \mathrm{i}\gamma\omega + \omega_0^2)} = \frac{(\omega_0^2 - \omega^2) + \mathrm{i}\gamma\omega}{m(\omega_0^2 - \omega^2)^2 + \gamma^2\omega^2}. \tag{3}$$

The fluctuation–dissipation theorem connects the power spectrum of the thermal fluctuations $|u|^2$ to the imaginary part of the susceptibility with $|u|^2(\omega) = kT\chi''(\omega)/\pi\omega$. With this relation we get

$$|u|^2(\omega) = \frac{kT}{\pi\omega}\chi''(\omega) = \frac{A\gamma}{(\omega_0^2 - \omega^2)^2 + \gamma^2\omega^2} \tag{4}$$

with the oscillator strength $A = kT/\pi m$, where k is the Boltzmann constant and T the temperature.

The noise spectrum thus has the form of a Lorentzian. For a spherical text body (see figure 1), the damping constant γ is

$$\gamma = \frac{\zeta}{m} = \frac{6\pi\eta r}{m} \tag{5}$$

with ζ the friction coefficient, η the viscosity of the ambient medium and r the hydrodynamic radius of the sphere. For a real cantilever, these quantities have to be replaced by effective quantities. The cantilever is a three-dimensional body with acoustic eigenmodes. The shape is such that the lowest eigenfrequency ('fundamental') is much lower than all other eigenfrequencies. In the following, we confine ourselves to the behaviour of the fundamental mode. We fit the data with a Lorentzian with eigenfrequency ω_0, damping constant γ and the oscillator strength $A = kT/\pi m$. The effective parameters κ, m and ζ can be evaluated according to

$$m = \frac{kT}{\pi A} \tag{6a}$$

$$\zeta = \gamma\frac{kT}{\pi A} \tag{6b}$$

$$\kappa = \omega_0^2\frac{kT}{\pi A}. \tag{6c}$$

This analysis can in principle be made for all eigenmodes of the cantilever, yielding different effective parameters for the different modes.

Interactions with the environment will affect the noise spectra. The interaction can be modelled by a change in the effective parameters κ, ζ and m. The changes correspond to elastic coupling, viscous coupling and certain 'trapped mass'. The trapped mass takes part in the movement and therefore contributes to the inertia of the system. The term 'trapped' does not imply a rigid attachment to the cantilever. In particular the inertia of the system may change when the pattern of flow changes.

Changes in the spectra are expected not only when the ambient medium changes but also when the cantilever approaches a solid surface. For separations smaller than the dimensions of the cantilever, the flow pattern will be altered, resulting in coupling. Güthner *et al* [9] have assessed the coupling strength within a very simple model. They consider a flat circular plate of radius L which is mounted parallel to the surface at a distance z and oscillates in the z direction. If $L \gg z$ and if the medium is incompressible, the friction coefficient is given by

$$\zeta(z) = \zeta_\infty + \frac{3\pi\eta L^4}{4}\frac{1}{z^3}. \tag{7}$$

Note that equation (7) assumes that $L \gg z$ so that we do not expect to find a z^{-3} power law for $\gamma(z)$ over the entire range of z. Equation (7) can be used to assess the range z_h of hydrodynamic interactions. They will be appreciable whenever the second term in equation (7) is comparable with the friction at infinite distance ζ_∞. ζ_∞ can be taken to be about the value for a sphere (equation (5)) with the hydrodynamic radius L, i.e. $\zeta_\infty \approx 6\pi\eta L$. This gives a range $z_h \approx L$. Indeed we find that, in water, the range of hydrodynamic effects is $z_h \approx L$. In air, however, the range is shorter. We suspect that ζ_∞ in air is not dominated by hydrodynamic friction but rather by internal friction of the cantilever. In this case, ζ_∞ is much larger than $6\pi\eta L$ and the second term of equation (7) competes with ζ_∞ only at lower values of z.

Finally we assess the minimal time needed in order to obtain meaningful data. We require that the frequency resolution should be 1% of the resonance frequency. By virtue of the sampling theorem, we can obtain one data set in a time $T = 100\pi/\omega_0 \approx 5$ ms. Since the thermal noise is a Gaussian process, the standard deviation on one individual data point will be the same as the expectation value. In order to improve the accuracy to 3%, 1000 data sets are needed, which gives a data acquisition time of about 5 s. Indeed, we could achieve reasonable data quality within a couple of seconds. Noise measurements therefore easily allow for the determination of viscoelastic profiles as a function of cantilever height, z, within some minutes.

3. Experimental set-up and data analysis

We used the commercial instruments Nanoscope II (Digital Instruments) and TMX 2010 (Topometrix). In both instruments, the deflection of the cantilever is detected by an optical lever technique. The scanner was only used as a sample holder. No scanning in the x–y plane was performed and the feedback circuit was unplugged.

Since we observe electronic $1/f$ noise at frequencies below 2 kHz, we discard all data below that frequency. We used V-shaped silicon nitride cantilevers form Digital Instruments, which were gold coated on the back. Measurements shown in one plot were all made with the same cantilever.

We found that different cantilevers show appreciable variability in resonance frequency and spring constant even if they are of the same type [17, 18]. The scanning force microscope was installed in a vacuum chamber with a minimum pressure of 10 Torr. A variety of different gases were used. A liquid cell was available as well.

The noise data were obtained in the following way. The signal was read out in the 'force' mode with the highest scan rate available. No actual scanning occurred, however, because the scanner was unplugged. The resulting picture contains only noise. The power spectrum was obtained as the square modulus of the Fourier transform of these data. In the Nanoscope II instrument, the signal is normalized to the laser intensity so that laser fluctuations cancel out. The highest accessible frequency of about 32 kHz is determined by the sampling rate. We checked for aliasing. The frequency resolution depends on the length of the data strings transformed. We mostly used strings of 512 points, yielding a frequency resolution of 64 kHz. The frequency calibration was checked by acoustically exciting the cantilever with a known frequency. We averaged the power spectrum over three pictures corresponding to an overall measurement time of 4 s.

The relative distance between the cantilever and the sample was changed by a computer-controlled stepper motor which varies the height of the scanning force microscope head. Once the cantilever is in contact with the sample surfaces, it sticks to the surface even when the cantilever holder is retracted. To avoid this adhesion, the distance dependence of the noise spectra is measured during approach. The point of contact is detected as a sharp increase in the DC signal. All distances are referenced to this point of contact. The smallest steps were 100 nm. We estimate the statistical error to be about 50 nm. However, the distance between the sample and the tip differs from the effective hydrodynamic distance between the sample and the cantilever by about the tip height (2.9 μm). In this respect our distance data can only be an estimate of the effective distance.

4. Results and discussion

To obtain confidence in our model, we performed measurements in an ethanol–water mixture without any surface present. We varied the viscosity by varying the ethanol weight fraction. The values for the viscosity η were taken from the *CRC Handbook* [15]. Figure 2 shows the noise spectra. The power spectra were fitted with a Lorentzian. The fits improved when we allowed for a constant offset. For the fits shown in figure 2, we confined the fitting range to a region around resonance.

In some situations, significant discrepancies between the fits and the data appeared when the fitting range was extended to the full data range. This occurred more often in liquids than in gases. For very large damping, as we observe in liquids, the resonance curves become quite asymmetric. The quality factor Q can be derived either from the ratio of the peak maximum to the DC limit or from the width of the peak. In liquids, the quality factors derived in these two ways do not always quite agree. The band width indicates a lower Q-factor than the peak-to-DC ratio. The fitting routine tries to provide a compromise.

Ordinary $1/f$ noise cannot be at the origin of this discrepancy, because $1/f$ noise would induce spurious asymmetries rather than artificially reducing them. We believe that 'multiplicative' noise is responsible for the observed discrepancies. The noise, induced by fluctuations in the amplification electronics or fluctuations in the optical part of the device, not only is additive to the thermal noise but also has a multiplicative part. Because this noise enters as a multiplicative factor, it will convolute into the noise spectra. Low-frequency multiplicative noise will broaden all the peaks in the data. It can therefore explain why our data seem to have band widths, which are systematically large. Correcting for this error is

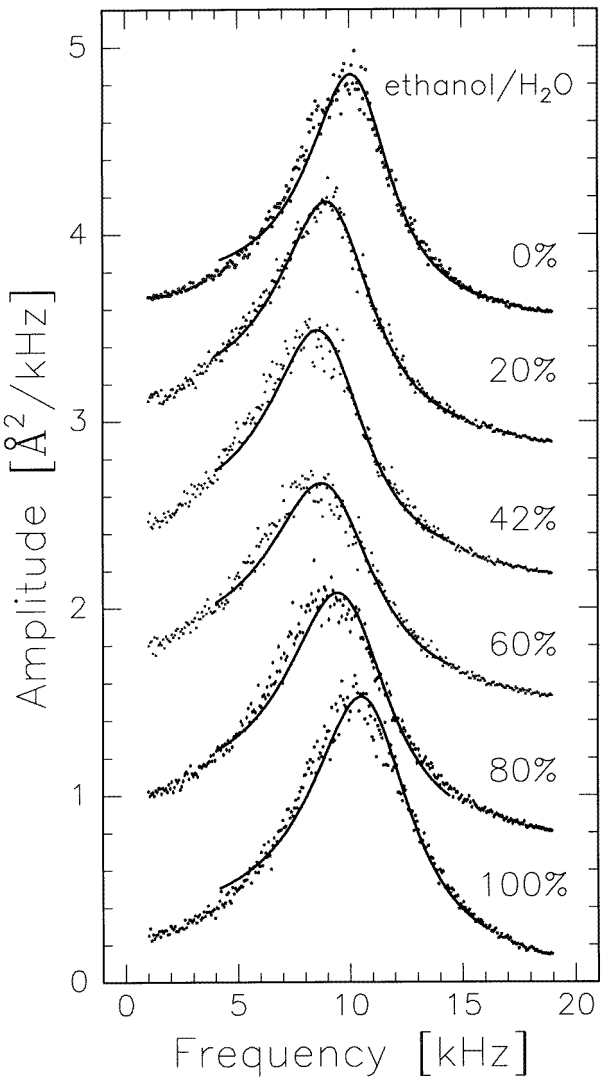

Figure 2. Noise spectra for various weight fractions of ethanol in water. The solid curves are fits to a Lorentzian. The viscosity does not depend linearly on the ethanol concentration but has a maximum around 42%, whereas the density slowly decreases with increasing ethanol concentration. The amplitude was calibrated with a conversion factor derived from the slope of the 'force–distance curve'. The spectra are shifted by an arbitrary but constant offset.

difficult, because the DC limit of our noise spectra is poorly defined also. This region is masked by additive $1/f$ noise. We therefore cannot derive the Q-factor from the peak-to-DC ratio in a reliable way. We therefore decided to apply no correction at all and to confine the fitting range around the resonance. The above discussion should be kept in mind as a caveat. We estimate that systematic errors induced by multiplicative noise are on the 10% level. Moreover they are not expected to vary with the other experimental parameters.

The noise amplitude can be calibrated with a conversion factor determined from the slope

of the so-called 'force–distance curve' (detector signal versus z peizo position) in the linear contact regime [16]. From the calibrated noise spectra we derive the effective constants m_{eff}, κ_{eff} and γ_{eff} with equations (6*a*)–(6*c*). For noise spectra taken without any additional elastic forces present, κ is just the spring constant of the cantilever. There is conceptual similarity to the work by Hutter and Bechhoefer [16], who derived the spring constant from the integrated noise. From the fit we obtain $\kappa \approx 0.021$ N m^{-1}. When we derive the spring constant from the integrated noise [16] using $\langle z^2 \rangle = kT/\kappa$ (equipartition theorem) we obtain $\kappa \approx 0.037$ N m^{-1}. We do not apply the correction factor of 4/3 to the equipartition theorem suggested by Butt and Jaschke [20], because our limited range of integration eliminates the influence of all higher harmonics. Both values for κ are significantly lower than the value of $\kappa = 0.58$ N m^{-1} given by the manufacturer. The manufacturer quotes a thickness of the cantilever of 0.6 μm. The large discrepancy is probably due to a real thickness of the cantilevers less than 0.6 μm. The spring constant depends on the third power of the thickness. We calculated the spring constant from the exact solution for the V-shaped cantilevers based on a finite-element analysis [21] with the given geometry and the elastic modulus $E = 1.5 \times 10^{11}$ N m^{-2} [12] of Si_3N_4 and found that $\kappa = 0.20$ N m^{-1} for a thickness of 0.6 μm. To be consistent with our experimental data, a thickness of 0.32 μm had to be assumed. At this point, we do not know whether this is reasonable. Other factors decreasing the resonance frequency may be geometrical irregularities such as notches. Spring constants significant lower than values predicted by theory have been reported before ([17–20], and references therein). Errors in the determination of the absolute spring constant will not effect our subsequent discussion of the change in the spring constant in changing environments.

Figure 3 shows the derived oscillator strengths $A(c)$, the eigenfrequencies $f_0(c)$ and the damping constants $\gamma(c)$ as functions of the ethanol weight fraction c. Note that the viscosity is not a linear function of the ethanol content but has a maximum around $c = 42\%$. The density on the other hand decreases monotonically. We therefore plot the derived parameters m_{eff}, κ_{eff} and ζ_{eff} versus η rather than ethanol weight fraction c (figure 4). The spring constant κ_{eff} is roughly independent of the viscosity, i.e. there is no elastic coupling. As expected, the fraction coefficient ζ increases linearly with increasing viscosity. The effective mass m increases with both increasing density and increasing viscosity. To distinguish between the two effects, the effective volume $V_{eff} = m_{eff}/\rho$ is calculated and a linear increase in V_{eff} with increasing viscosity is found. That is assumed to be due to a changing flow pattern with changing viscosity.

Note that the friction coefficient is not proportional to the viscosity. Instead, a straight line through our data points has quite a high offset. This offset may be due to internal friction. On the other hand, the hydrodynamic situation may be more complicated than suggested in equation 5.

The following experiments were performed with a Nanoscope II instrument. Since amplitude calibration is quite a tedious process and since we focus on the changes in parameters rather than on absolute values, we did not perform an amplitude calibration for each data set. Rather, we assumed a certain spring constant for infinite distances. The amplitude calibration derived in this way is of course only correct to the extent to which the assumed spring constants are correct. We used spring constants calculated according to the scheme described in [21]. In the following, we describe the changes in parameters upon approach to a surface. The following comparisons were made: in section 4.1, the approach in nitrogen versus the approach in water; in section 4.2, the approach in nitrogen at various pressures; in section 4.3, the approach at ambient pressure in nitrogen, argon and helium; in section 4.4, the approach at different inclinations of the z direction relative to the surface normal; in section 4.5, the approach to a hard surface versus the approach to a soft surface.

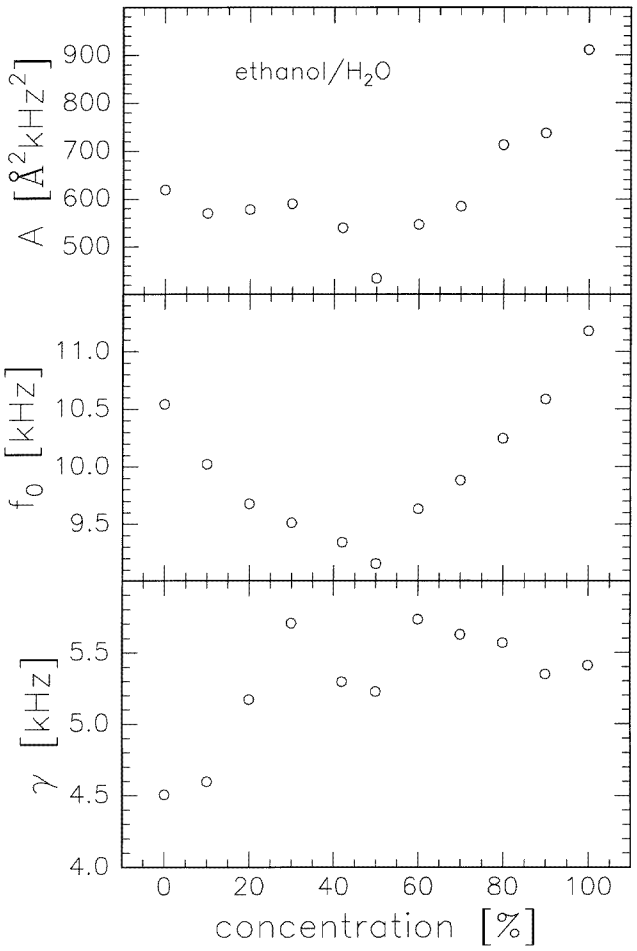

Figure 3. Oscillator strength $A(c)$, eigenfrequency $f_0(c)$ and damping constant $\gamma(c)$ as functions of the ethanol content in H_2O. The maximum of the viscosity is reached at around 42% ethanol.

4.1. Approach in nitrogen and water

Figure 5 displays distance-dependent noise during the approach to a graphite surface in N_2. At a separation of about 5 μm the amplitude starts to decrease, the peak broadens and the resonance $f_{res} = (f_0^2 - \gamma^2/2)^{1/2}$ shifts to lower values. Figure 6 shows the noise spectra during the approach to a surface in water. In both plots we have included noise spectra in contact. In the case of contact, the apparent mass is very high because the sample is tightly coupled to the cantilever. Therefore the amplitude of oscillation drops below our level of sensitivity. Note that we can clearly distinguish 'contact' and a highly overdamped situation such as the one that we observe in water for small distances. In water, the damping during approach is much stronger and the interaction range is much longer that in N_2. The solid curves in figures 5 and 6 show the fits to a Lorentzian (equation (4)).

All curves within one ambient medium could be well fitted with a constant oscillator strength A and a constant eigenfrequency f_0. Apparently, both the effective mass and the

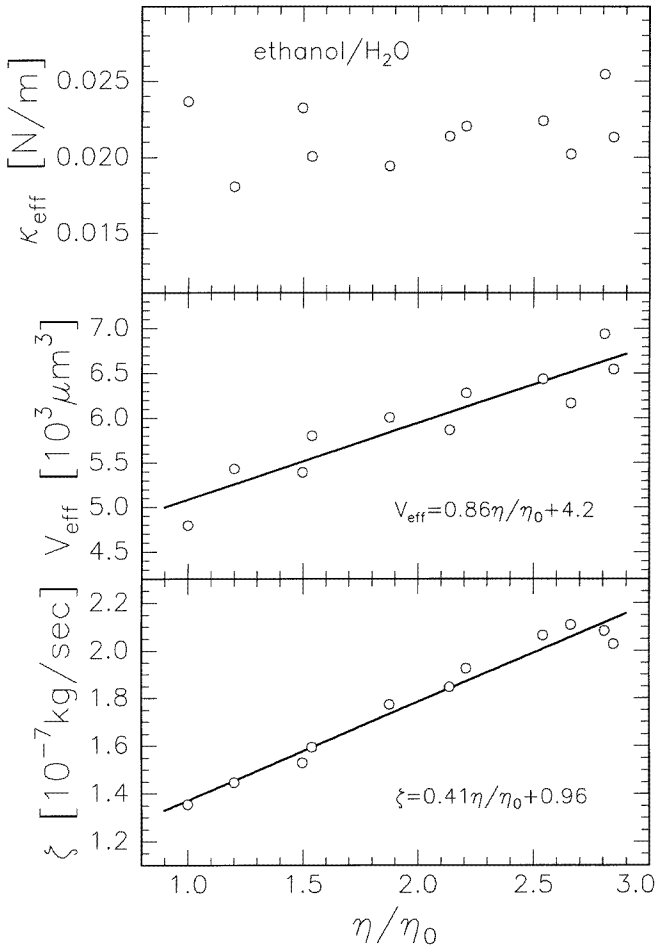

Figure 4. Effective spring constant κ_{eff}, effective volume V_{eff} and friction coefficient ζ as functions of the relative viscosity η/η_0 (η_0 is the viscosity of water at 20 °C). The effective mass depends on both the density ρ and the viscosity. To show the influence of the viscosity alone, the effective volume $V_{eff} = m_{eff}/\rho$ is calculated. The solid curves are linear fits.

spring constant remain approximately constant. All the changes are due to viscous coupling.

In water the effective mass is higher than in air by a factor of about 20. The friction coefficient is much higher as well because the viscosity of water is much higher than that of N_2 (figure 7). Indeed, if we divide the change $\zeta(z) - \zeta_\infty$ in friction coefficient by the viscosity of the medium, the data from N_2 and water collapse to a single curve (figure 8). The hydrodynamic interaction therefore scales with viscosity. Scaling of the interaction with viscosity was predicted by the simple model used by Güthner *et al* [9] (equation (7)). However, this model also predicts that the interactions scale with distance like z^{-3}. Our data do not support that scaling law. Instead we find an exponent close to 1. The reason certainly is geometrical. A cantilever looks very different from a circular plate.

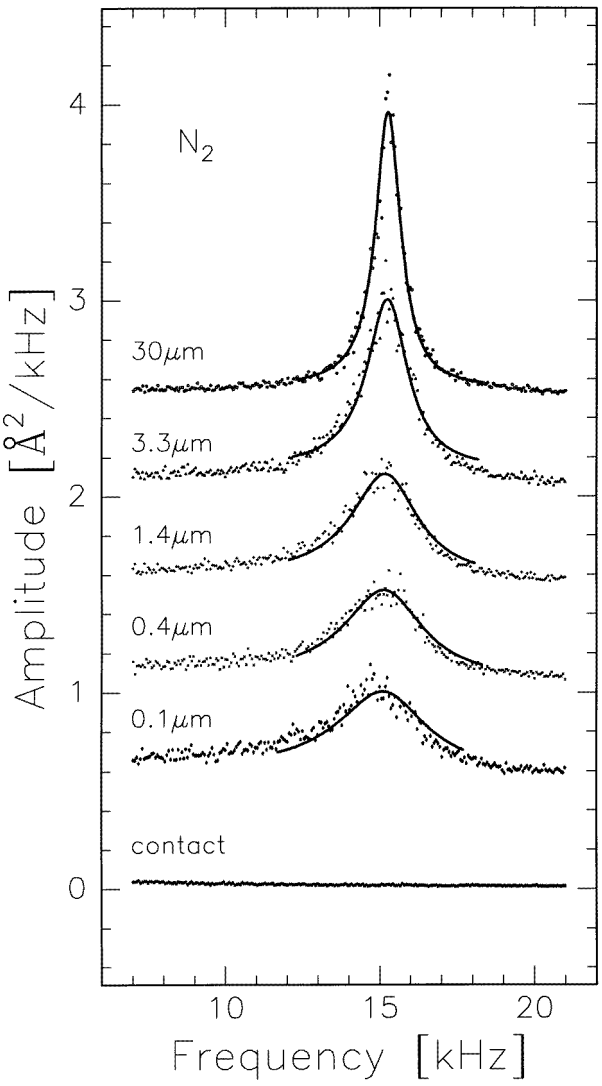

Figure 5. Noise spectra and fits (solid curves) in N_2 at ambient pressure during the approach of the cantilever to the surface. The amplitudes are shifted by an arbitrary but constant offset. The amplitudes were calibrated with a conversion factor derived from a calculated spring constant according to [21].

4.2. Approach in nitrogen at various pressures

Figure 9 shows the distance dependence of the resonance frequency $f_{res}(z) = (f_0^2 - \gamma^2(z)/2)^{1/2}$ and the friction coefficient $\zeta(z)$ calculated from the fit parameters f_0, $\gamma(z)$ and κ for various pressures of N_2. The corresponding effective masses are listed in the inset. As expected, the effective mass decreases with decreasing pressure. The decrease in m_{eff} is mainly responsible for the increase in $f_{res}(z = \infty)$ at infinite distance. Only small variations in $\zeta(z = \infty)$ were found.

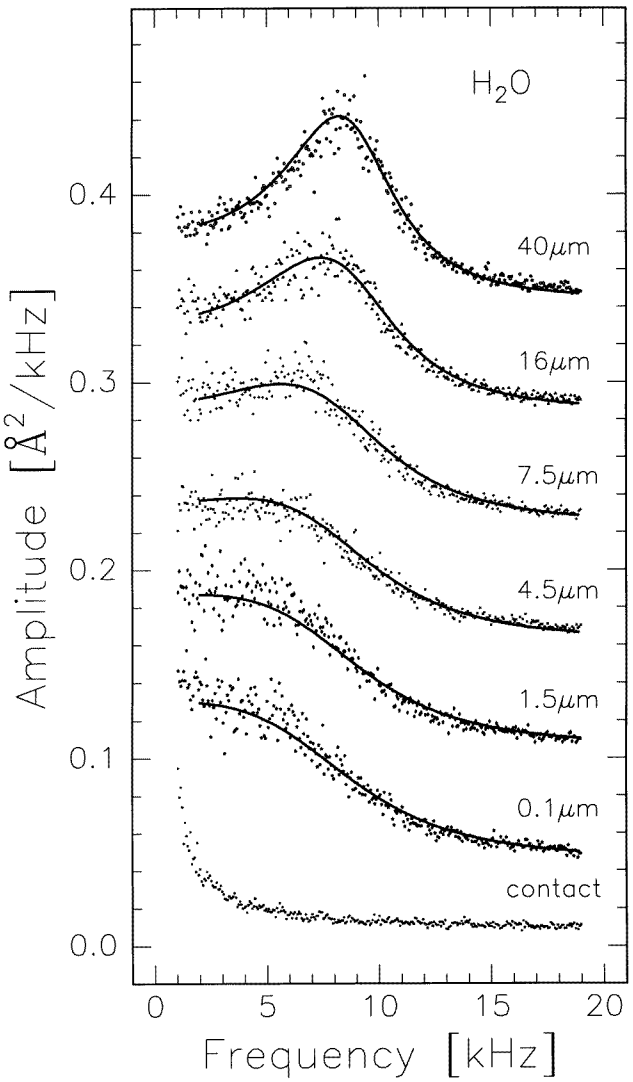

Figure 6. Noise spectra and fit (solid curves) in H_2O during the approach of the cantilever to the surface. The amplitudes are shifted by an arbitrary but constant offset. The amplitudes were calibrated with a conversion factor derived from a calculated spring constant according to [21].

If we divide the difference in effective mass between 760 and 10 Torr by the density of N_2, we can calculate a 'trapped volume'. We find a volume of 1300 μm^3. If we set the area of the cantilever to be about 13 000 μm^2, we find an effective thickness of the 'trapped volume' on both sides of the cantilever of about 50 nm.

The friction coefficient $\zeta(z)$ does not vary much with pressure unless the pressure drops to about 10 Torr. This is consistent with the hypothesis that viscous coupling depends on viscosity alone. The viscosity of gases is largely independent of pressure as long as the mean free path is shorter than the range of interaction [22]. The mean free path b is given by $b = 1/(2^{1/2}\pi n d^2)$ [22] with $n = p/kT$ the number density and p the pressure.

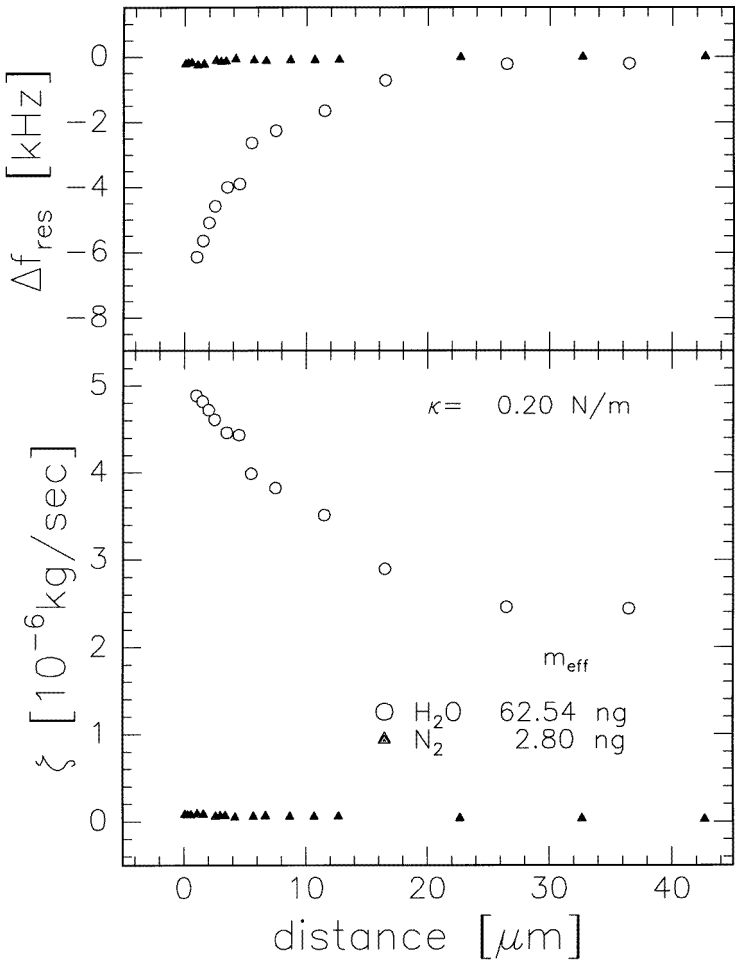

Figure 7. Shift of the resonance frequency $\Delta f_{res}(z) = f_{res}(\infty) - f_{res}(z)$ and friction coefficient $\zeta(z)$ calculated from the fit parameters versus distance z in water and N_2. The resonance frequency at infinite distance $f_{res}(\infty)$ shifts from 42.5 kHz in N_2 to 8.2 kHz in water.

Inserting the molecular diameter $d \approx 3$ Å and equating the mean free path to 10 μm, we find a pressure of 10 Torr, below which the effective viscosity decreases. Indeed we find a significantly lower coupling at a pressure of 10 Torr only.

4.3. Approach at ambient pressure in nitrogen, argon and helium

To check for the dependence of the hydrodynamic coupling on the ambient medium, we used a variety of different gases. The different densities of the gases cause different effective masses, leading to a variation in $f_{res}(z = \infty)$ at infinite distance. As for the range of the hydrodynamic interaction, we do not find significant differences in the friction coefficients for the different gases. This implies that the range of interaction depends only weakly on density and therefore also depends only weakly on the speed of sound, the values of which are quite different in the different gases. This result—although surprising at first glance—

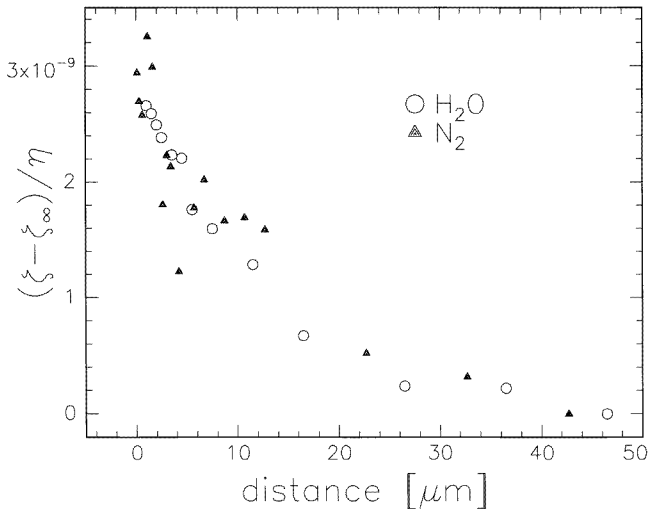

Figure 8. The distance-dependent part of the friction coefficient $\zeta(z) - \zeta(\infty)$ divided by the viscosity of the ambient medium versus distance z. The data sets collapse onto one curve.

confirms the model of Güthner *et al*, claiming viscosity to be the determining factor. The viscosities are quite similar for the different gases.

4.4. Approach at different inclinations of the z-direction relative to the surface normal

If one wishes to diminish the hydrodynamic coupling, two approaches seem viable: decreasing the viscosity η by going to low pressures and decreasing the effective radius (L in equation (7)) by using a cantilever that is sharply pointed on the scale of some microns. In an initial experiment, we decreased the effective diameter of the cantilever by using it at an inclined angle. In this way, only the front edge of the cantilever interacts with the surface. The viscous coupling decreased as expected, while the effective mass remained unchanged.

If we consider very large tilt angles, the situation changes qualitatively, because the motion of the cantilever with respect to the sample is no longer a vertical but rather a lateral displacement. A rough estimate shows that $\zeta(z)$ for this geometry should be

$$\zeta(z) \approx \zeta_\infty + \eta L^2 \frac{1}{z}. \tag{8}$$

Inserting $\eta \approx 10^{-3}$ Pa s, an effective cantilever radius of 10 μm and an effective mass of 5 ng we find that $\gamma(10\ \mu\text{m}) - \gamma_\infty \approx 2$ kHz compared with 19 kHz from equation (7). The advantage of measuring in the shear mode rapidly increases when the distances become smaller. The example shows that it should indeed be possible to overcome hydrodynamic interactions and to measure very local viscoelastic properties of a surface. Unfortunately, we cannot measure at such a high inclination with the existing set-up.

4.5. Approach to a hard surface versus approach to a soft surface

Finally we performed exploratory experiments, where we compare the viscoelastic coupling to a hard surface with that to a soft surface. The hard surface was bare glass. The soft

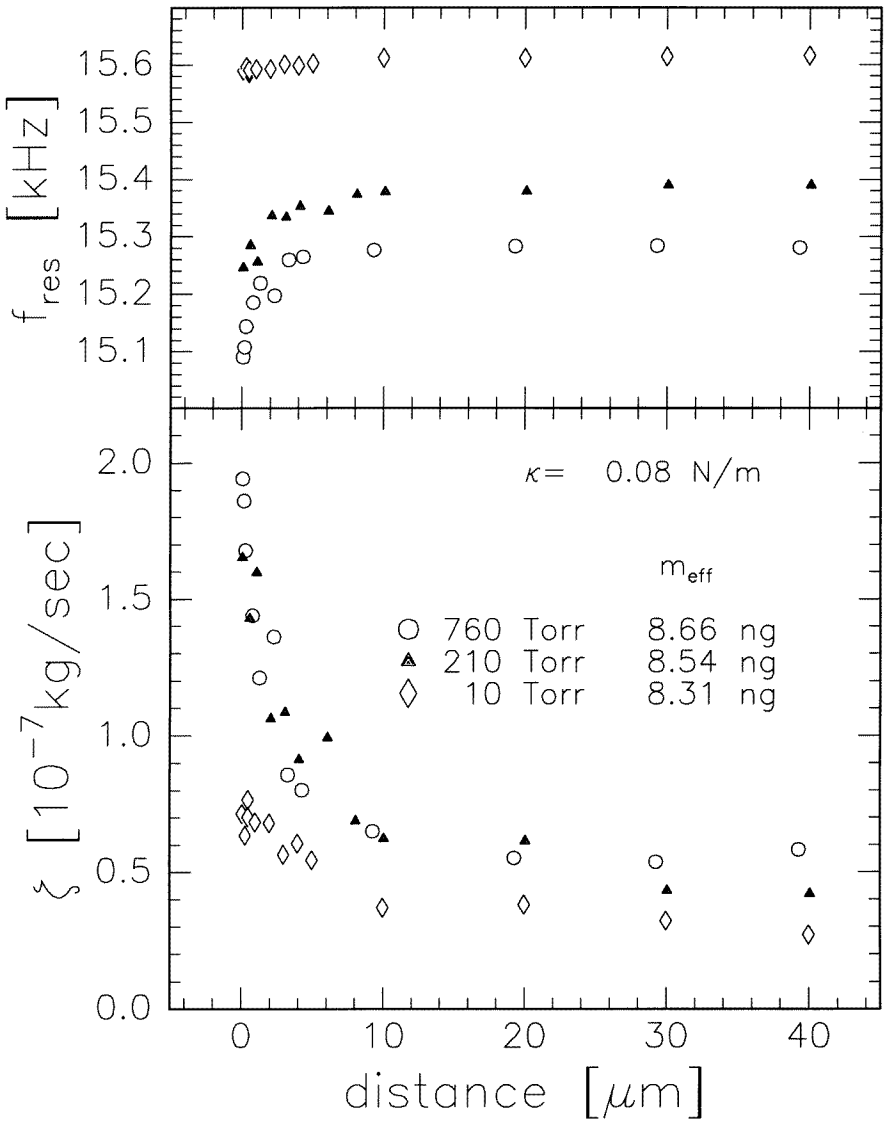

Figure 9. Resonance frequency $f_{res}(z)$ and friction coefficient $\zeta(z)$ in gaseous N_2 calculated from the fit parameters versus distance z for various pressures.

surface was a thin polymer brush of poly(methyl methacrylate) (PMMA) grafted from a SiO_x surface [23]. These samples are very convenient for SFM measurements, because the material is covalently attached to the substrate and cannot be detached during experiment. The samples have undergone extensive Soxhlet extraction prior to measurement in order to remove all material not covalently bound. Brushes swollen in a solvent are therefore very soft or even fluid systems while at the same time being held in place by the chemical bond.

The thickness of the PMMA layer in air was 80 nm, as determined by surface plasmon spectroscopy. The experiments were performed in toluene, which causes PMMA to swell,

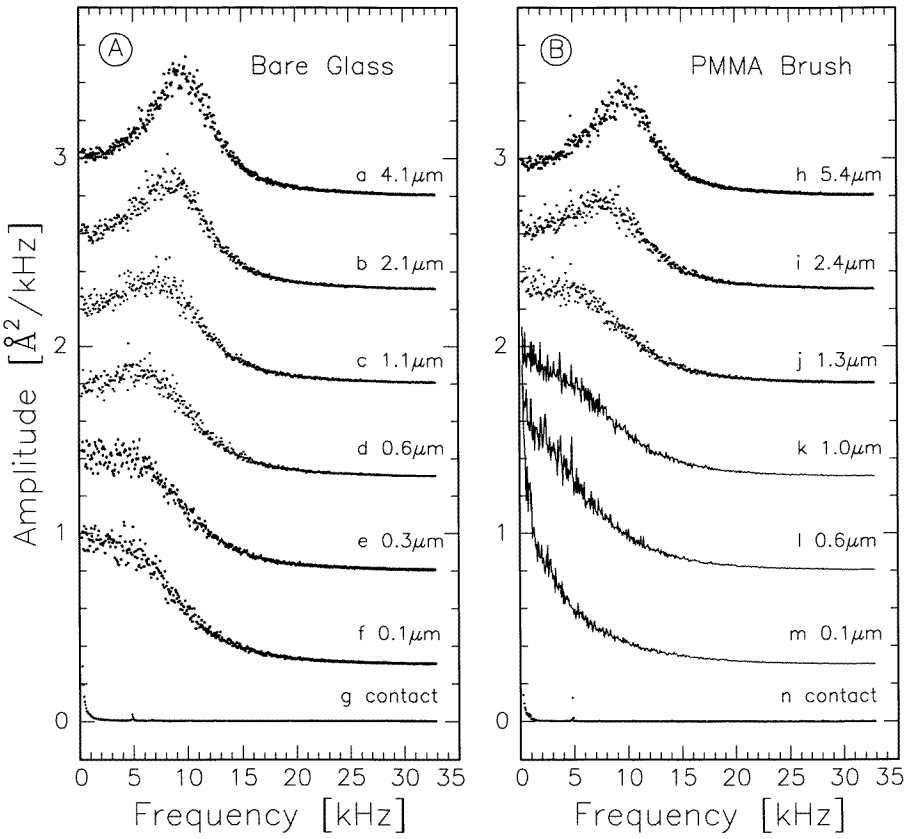

Figure 10. Noise spectra for the approach to (*a*) a bare glass surface and (*b*) glass covered with a covalently bound PMMA brush in toluene. The amplitudes were calibrated with a conversion factor derived from the slope of the 'force–distance curve'. The data were vertically shifted by an arbitrary but constant offset. When the tip is immersed into the swollen PMMA brush (solid curves in (*b*)), the spectra are significant different from the spectra for approach to bare glass (*a*).

so that the PMMA layer is expected to be much softer than the glass reference.

The noise spectra are shown in figure 10. For glass (figure 10(*a*)), changes in the noise spectra due to the hydrodynamic damping described above are observed. The change between the highly overdamped situation (f) and the point of contact (g) is discontinuous. We did not observe spectra intermediate to f and g.

The spectra of the PMMA brush also show hydrodynamic damping comparable with glass for separations from the substrate larger than 1.3 μm. For separations less than 1.1 μm, the spectra are significantly different from the spectra for glass. These noise spectra are shown as solid curves k, l, and m in figure 10(*b*). The noise decreases and is limited to very low frequencies. This corresponds to an increase in damping well beyond the values observed for ordinary hydrodynamic coupling to a bare glass substrate. Detailed analysis shows that the effective spring constant increases as well. The distance regions where the tip movement slows down coincides with the region where static repulsion starts as seen in the so-called 'force–distance curve'.

Note that the transition from a highly overdamped situation to the 'contact' with vanishing noise is again discontinuous (figure 10(*b*), m and n). Our data suggest that the tip is able to penetrate through the brush until it hits the hard glass surface. This finding is quite plausible when the rather strong swelling of the polymer brush in solvent is considered [24]. A swelling by a factor of at least 3 is deduced from the 'force–distance curve' as well. Apparently, the segment density inside the brush is of the order of 30%, which allows the tip to dive into the brush quite easily. More details will be provided in a subsequent publication.

5. Conclusions and outlook

We have analysed the noise spectra of a scanning force microscope tip during the approach to a surface in different gaseous and liquid media. We fit the noise spectra with an effective mass, an effective spring constant and a friction parameter and show that it is possible to discriminate between viscous coupling and elastic coupling and changes in the effective mass. During the approach to a surface, only the friction parameter varies while the effective mass and the spring constant remain constant. The results are compatible with simple models of the hydrodynamic interaction between the cantilever and a surface. By observing the difference between the noise spectra of a scanning force microscope tip in contact with a hard surface and a polymer brush, we could show that the method is in fact sensitive to the local dynamic properties of the surface.

The method described can have a great potential for measuring the local dynamical properties of interfaces. Although the method is slow compared with other methods, it allows for quantitative analysis and has vertical resolution.

When the coupling is large, the resonance frequency $\omega_{res} = (\omega_0^2 - \gamma^2/2)^{1/2}$ will become purely imaginary. That may be an unfavourable situation for experiment. In order to be able to observe large couplings, one needs to keep the ratio of γ to ω_0 small. We have

$$\frac{\gamma}{\omega_0} = \frac{\zeta}{\sqrt{\kappa m}} = \frac{\zeta}{Z}. \tag{9}$$

The quantity Z is the mechanical impedance of the cantilever. Conventional cantilevers are designed with a low impedance in order to minimize the effects of thermal noise. Clearly, this is not the optimal design for the detection of noise, which is the goal of this work. In order to increase the impedance, one needs to increase the mass and the spring constant at the same time, thereby leaving the resonance frequency unchanged.

Although imaginary resonance frequencies are unfavourable, they are not necessarily prohibitive for data analysis. Our data show that an analysis of the noise is still possible in overdamped situations. We do not rely on oscillatory movement in the same way as active measurement schemes do. Overdamped situations may in fact be easier to analyse because the fitting parameter ω_0 can possibly be eliminated. Thus one may try to perform experiments in the limit of very small impedances Z, where the cantilever motion is dominated by friction. The cantilever essentially follows the Brownian motion of its environment. It remains to be seen whether this limit can be achieved.

Acknowledgments

We would like to thank Christian Hahn and Masahiko Hara from the Institute of Physical and Chemical Research (RIKEN) for support and helpful discussions. Hans-Jürgen Butt has made very valuable comments. Jürgen Rühe and Martin Schimmel

have provided the PMMA brushes. Part of this work was performed at RIKEN (Wako-shi, Japan). The Deutsche Akademischer Austauschdienst supported this work with a 'Doktorandenstipendium aus Mitteln des zweiten Hochschulsonderprogramms'.

References

[1] Binnig G, Quate C F and Gerber C 1986 *Phys. Rev. Lett.* **56** 930
[2] Mailvald P, Butt H-J, Gould S A C, Prater C B, Drake B, Gurley J A, Elins V B and Hansma P K 1991 *Nanotechnology* **2** 103
[3] Radmacher M, Tillmann R W, Fritz M and Gaub H E 1992 *Science* **257** 1900
[4] Radmacher M, Tillman R W and Gaub H E 1993 *Biophys J.* **64** 735
[5] Kajiyama T, Tanaka K, Ohki I, Ge S-R, Yoon J-S and Takahara A 1994 *Macromolecules* **27** 7932
[6] Spatz J P, Sheiko S, Möller M, Winkler R G, Reineker P and Marti O 1995 1995 *Nanotechnology* **6** 40
[7] Florin E L, Radmacher M, Fleck B and Gaub H E 1994 *Rev. Sci. Instrum.* **65** 639
[8] Güthner P, Fischer U Ch and Dransfeld K 1988 *Beitr. elektronenmikroskop. Direktabb. Oberfl.* **21** 27
[9] Güthner P, Fischer U Ch and Dransfeld K 1989 *Appl. Phys.* B **48** 89–92
[10] den Boef A J 1989 *Appl. Phys. Lett.* **55** 439
[11] Martin Y, Williams C C and Wickramasinghe H K 1987 *J. Appl. Phys.* **61** 4723
[12] Sarid D 1991 *Scanning Force Microscopy* (Oxford: Oxford University Press)
[13] Reichl L E 1987 A *Modern Course in Statistical Physics* (London, TX: University of Texas Press)
[14] Kubo R, Toda M and Hashitsume H 1985 *Statistical Physics* vol 2 (Berlin: Springer)
[15] *CRC Handbook of Chemistry and Physics* 1985–6, 66th edn (Boca Raton, FL: CRC Press)
[16] Hutter J L and Bechhoefer J 1993 *Rev. Sci. Instrum.* **64** 1868
[17] Cleveland J P, Mane S, Bocek D and Hansma P K 1993 *Rev. Sci. Instrum.* **64** 403
[18] Butt H-J, Siedle P, Seifert K, Fendler K, Seeger T, Bamberg E, Weisenhorn A L, Goldie K and Engle A 1993 *J. Microsc.* **169** 75–84
[19] Butt H-J, Jaschke M and Ducker W 1995 *Bioelectrochem. Bioenergetics* **38** 191–201
[20] Butt H-J and Jaschke M 1995 *Nanotechnology* **6** 1
[21] Sader J E and White L 1993 *J. Appl. Phys.* **74** 1
[22] Herman M A and Sitter H 1989 *Molecular Beam Epitaxy* (Berlin: Springer) p 3
[23] Tovar G, Paul S, Knoll W, Prucker O and Rühe J 1995 *Supramol. Sci.* **2** 89
[24] Paul S 1995 *PhD Thesis* Universität Mainz